

See discussions, stats, and author profiles for this publication at: <https://www.researchgate.net/publication/221860772>

# Calibration of a Chemical Ionization Mass Spectrometer for the Measurement of Gaseous Sulfuric Acid

ARTICLE in THE JOURNAL OF PHYSICAL CHEMISTRY A · FEBRUARY 2012

Impact Factor: 2.69 · DOI: 10.1021/jp212123n · Source: PubMed

---

CITATIONS

11

---

READS

23

## 4 AUTHORS, INCLUDING:



[Andreas Kürten](#)

Goethe-Universität Frankfurt am Main

62 PUBLICATIONS 1,149 CITATIONS

[SEE PROFILE](#)



[Linda Rondo](#)

Goethe-Universität Frankfurt am Main

34 PUBLICATIONS 504 CITATIONS

[SEE PROFILE](#)



[Joachim Curtius](#)

Goethe-Universität Frankfurt am Main

155 PUBLICATIONS 2,720 CITATIONS

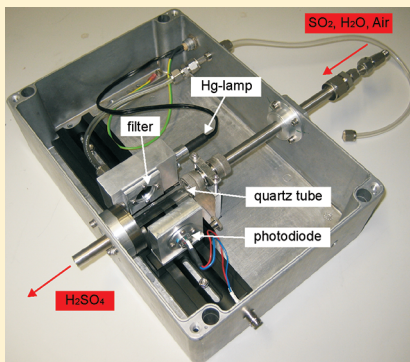
[SEE PROFILE](#)

# Calibration of a Chemical Ionization Mass Spectrometer for the Measurement of Gaseous Sulfuric Acid

Andreas Kürten,\* Linda Rondo, Sebastian Ehrhart, and Joachim Curtius

Institute for Atmospheric and Environmental Sciences, Goethe-University Frankfurt am Main, Altenhöferallee 1, 60438 Frankfurt am Main, Germany

**ABSTRACT:** The accurate measurement of the gaseous sulfuric acid concentration is crucial within many fields of atmospheric science. Instruments utilizing chemical ionization mass spectrometry (CIMS) measuring  $\text{H}_2\text{SO}_4$ , therefore, require a careful calibration. We have set up a calibration source that can provide a stable and adjustable concentration of  $\text{H}_2\text{SO}_4$ . The calibration system initiates the production of sulfuric acid through the oxidation of  $\text{SO}_2$  by OH. The hydroxyl radical is produced by UV photolysis of water vapor. A numerical model calculates the  $\text{H}_2\text{SO}_4$  concentration provided at the outlet of the calibration source. From comparison of this concentration and the signals measured by CIMS, a calibration factor is derived. This factor is evaluated to be  $1.1 \times 10^{10} \text{ cm}^{-3}$ , which is in good agreement with values found in the literature for other CIMS instruments measuring  $\text{H}_2\text{SO}_4$ . The calibration system is described in detail and the results are discussed. Because the setup is external to the CIMS instrument, it offers the possibility for future CIMS intercomparison measurements by providing defined and stable concentrations of sulfuric acid.



## 1. INTRODUCTION

Aerosol particles formed by nucleation comprise a major part of the total aerosol load in the Earth's atmosphere. Their formation and growth have been observed at many different locations.<sup>1</sup> Aerosols have an important influence on the climate both through their direct interaction with electromagnetic radiation and their capability of acting as cloud condensation nuclei.<sup>2</sup> Model calculations suggest that about 50% of the globally averaged cloud condensation nuclei (CCN) originate from nucleated particles that have grown to CCN sizes.<sup>3</sup> The knowledge about vapors contributing to the formation of the clusters enabling the formation of new particles is still limited. However, field measurements show that sulfuric acid is a key compound and nucleation rates correlate with the concentration of sulfuric acid.<sup>4–7</sup> Recently, the nucleation of the binary sulfuric acid–water system under ultraclean conditions was studied in a chamber experiment by Kirkby et al.<sup>8</sup> and laboratory and chamber studies have shown that other compounds, like ammonia or oxidized organic substances, are capable of enhancing nucleation substantially.<sup>8–12</sup> Furthermore, studies of the cluster kinetics and thermochemistry for neutral and charged ion clusters containing  $\text{H}_2\text{SO}_4$  require measurement of the absolute gas phase concentration of sulfuric acid.<sup>13,14</sup> Sulfuric acid measurements have also been used to characterize UV photolysis systems by Kupc et al.<sup>15</sup> and to verify aerosol chamber flow and diffusion characteristics by Voigtländer et al.<sup>16</sup> Therefore, the accurate measurement of the sulfuric acid concentration is crucial during field, chamber, and other laboratory experiments.

For the measurement of gaseous sulfuric acid, chemical ionization mass spectrometers (CIMS) are widely used. These instruments have detection limits around  $1 \times 10^5$  molecules

$\text{cm}^{-3}$  for rather short integration times ( $\sim 1 \text{ min}$ ) and allow measurements in real time. The instruments make use of the selective proton transfer reaction between nitrate ions ( $\text{NO}_3^-$ ) and  $\text{H}_2\text{SO}_4$ . The rate for this reaction can be taken from the literature, however, it is subject to some uncertainty.<sup>17</sup> Therefore, the instruments are generally calibrated, which also allows taking into account the wall losses of  $\text{H}_2\text{SO}_4$  inside the CIMS inlet as well as the flow conditions inside the ion source where the nitrate ions are mixed with the sulfuric acid. This mixing introduces an uncertainty because the effective interaction time between the ions and the sulfuric acid in the sample gas is not known precisely. Therefore, different kinds of calibration methods have been developed that aim at introducing a known concentration of sulfuric acid into the CIMS and comparing the measured signals to the known concentration.

Within most calibration sources a gas mixture of air and water vapor is exposed to UV light from a mercury lamp (184.9 nm), which results in the photolysis of water vapor and the generation of OH radicals. This technique is utilized to calibrate CIMS instruments measuring OH and  $\text{HO}_2$  (see review by Dusanter et al.<sup>18</sup> and references therein). Through the addition of isotopically labeled  $\text{SO}_2$ , the OH is converted to  $\text{H}_2\text{SO}_4$ , which is then measured by CIMS. By using nonisotopically labeled  $\text{SO}_2$  instruments, measuring sulfuric acid can be calibrated as well. The challenge in calculating the resulting

**Special Issue:** A. R. Ravishankara Festschrift

**Received:** December 15, 2011

**Revised:** February 23, 2012

**Published:** February 24, 2012

concentration is to evaluate the exact value of the UV light intensity as well as the time over which the gas mixture is exposed to the UV light. These two parameters determine how much OH (and, therefore, H<sub>2</sub>SO<sub>4</sub>) will be produced for given gas concentrations and flow conditions. While some authors describe the direct measurement of the UV photon flux with a calibrated photodiode,<sup>19,20</sup> others derive the *It*-product (product of UV light intensity at 184.9 nm and effective illumination time) through chemical actinometry by using a known chemical reaction, for example, the conversion of N<sub>2</sub>O to NO<sub>x</sub>.<sup>21–23</sup> This latter method is used because the chemical species produced during the actinometry experiment can be measured easier than OH or H<sub>2</sub>SO<sub>4</sub>.

In this paper we describe a setup that can provide a known concentration of sulfuric acid, which is used to calibrate a CIMS instrument. The performance of this system has been tested with a CIMS from THS Instruments, LLC. The calibration source is an external stand-alone setup and is only connected when a calibration needs to be performed. This modular device allows connecting the calibration source to other CIMS instruments (in principle, also to instruments measuring OH). The system is described in detail and the results obtained are discussed. The purpose of the calibration system is to derive a factor that relates the measured ion signals (usually at *m/z* 62, NO<sub>3</sub><sup>−</sup> ion, and *m/z* 97, HSO<sub>4</sub><sup>−</sup> ion) to a true sulfuric acid concentration. We have tested whether this factor is constant over the entire range where H<sub>2</sub>SO<sub>4</sub> measurements with CIMS instruments have been reported (several 10<sup>5</sup> up to several 10<sup>9</sup> molecules cm<sup>−3</sup>). The value that was derived is constant over a wide range of concentrations but shows a deviation to lower values at lower nominally provided sulfuric acid concentrations. However, we have good reasons to assume that this dependency is an artifact intrinsic to our calibration system. Nevertheless, this finding could mean that for other calibration systems used a similar problem exists and can potentially lead to rather large errors in deriving sulfuric acid concentrations. This underlines the importance of discussing the performance and limitations of the H<sub>2</sub>SO<sub>4</sub> calibration system. It also shows that there is a need for future intercomparison measurements not only for different CIMS instruments but also with respect to the calibration systems used by different groups.

## 2. THEORY AND METHODS

**2.1. Sulfuric Acid Measurement by CIMS.** The detection of gaseous sulfuric acid through its reaction with NO<sub>3</sub><sup>−</sup>(HNO<sub>3</sub>)<sub>0–2</sub> primary ions has been described in detail by several authors.<sup>24,25</sup> Therefore, only a brief summary of the method is given here. The chemical ionization mass spectrometer used in this study was acquired from THS Instruments (THS Instruments LLC, U.S.A.). The previously installed americium source that was used to generate the primary ions has been replaced by a newly developed corona ion source. This source has been demonstrated to work reliably, giving low detection limits while having a negligible cross-sensitivity to SO<sub>2</sub>.<sup>26</sup> The sulfuric acid concentration can be calculated by relating the count rates, CR, at *m/z* 97 (HSO<sub>4</sub><sup>−</sup> ions) and *m/z* 64 (N<sup>18</sup>OO<sub>2</sub><sup>−</sup> ions):

$$[\text{H}_2\text{SO}_4] = \frac{1}{k \cdot t} \cdot \ln \left( 1 + \frac{\text{CR}_{97}}{166 \cdot \text{CR}_{64}} \right) \quad (1)$$

The factor 166 is used to account for the isotopic ratio between NO<sub>3</sub><sup>−</sup> and N<sup>18</sup>OO<sub>2</sub><sup>−</sup> ions. We generally use the isotope at *m/z*

64 because this yields a lower signal and avoids damage of the channeltron detector. The constant *k* for the reaction between the primary ions and the sulfuric acid is known from literature.<sup>17</sup> However, the reaction time *t* cannot be retrieved easily. In addition, losses within the CIMS ion source and the inlet occur, which have to be taken into account to relate the real sulfuric acid concentration to the measured signals. Therefore, the following relationship is used:

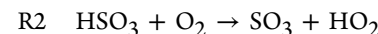
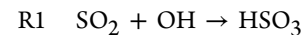
$$[\text{H}_2\text{SO}_4] = C \cdot \ln \left( 1 + \frac{\text{CR}_{97}}{166 \cdot \text{CR}_{64}} \right) \quad (2)$$

The factor *C* is a calibration factor that relates the measured signals to the true H<sub>2</sub>SO<sub>4</sub> concentration within the sample flow that enters the CIMS instrument. This factor is derived from the following calibration measurements:

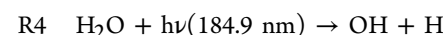
$$C = \frac{[\text{H}_2\text{SO}_4]_{\text{modeled}}}{\ln \left( 1 + \frac{\text{CR}_{97}}{166 \cdot \text{CR}_{64}} \right)} \quad (3)$$

While the denominator in this equation stems from the measurements during a calibration, the numerator is the result of a model calculation that is based on the calibration source measurements. In the following sections, the relevant methods and the theory used to derive the parameters that enter the model calculation are introduced, as well as the setup of the calibration system.

**2.2. Sulfuric Acid Production.** Within the calibration system, sulfuric acid is produced from SO<sub>2</sub> in the presence of OH, O<sub>2</sub>, and H<sub>2</sub>O. The formation of H<sub>2</sub>SO<sub>4</sub> is described by the following reaction scheme:<sup>27</sup>



The corresponding reaction rates are listed in Table 1. While the gases SO<sub>2</sub>, O<sub>2</sub>, and H<sub>2</sub>O are added to the calibration system at known concentrations through calibrated mass flow controllers (see section 3.1), OH is produced in situ through the photolysis of H<sub>2</sub>O under the presence of UV light at 184.9 nm:



The concentration of OH from this photolysis reaction can be calculated with the following equation:

$$[\text{OH}] = I \cdot t_r \cdot \sigma_{\text{H}_2\text{O}} \cdot \Phi_{\text{H}_2\text{O}} \cdot [\text{H}_2\text{O}] \quad (4)$$

Here, *I* denotes the photon intensity (amount of photons per second and per cm<sup>2</sup>), *t<sub>r</sub>* is the reaction or illumination time, σ<sub>H<sub>2</sub>O</sub> is the absorption cross section of water vapor, and Φ<sub>H<sub>2</sub>O</sub> is the quantum yield. For further discussion, the product of *I* and *t<sub>r</sub>* will be used and this quantity will be denoted as the *It*-product. The quantum yield for reaction R4 at 184.9 nm is 1.0, and the absorption cross section is 7.22 × 10<sup>−20</sup> cm<sup>2</sup> (cf. Table 1).<sup>28,29</sup> The water vapor concentration in eq 4 depends on the temperature *T*, the saturation vapor pressure of water *p<sub>sat</sub>*, and

**Table 1.** Reaction Rates, Photochemical Yields, Absorption Cross Sections, and Diffusion Coefficients Used to Model the H<sub>2</sub>SO<sub>4</sub> Concentration

reaction or parameter	value or expression	reference
R1, $k_1$	$1.3 \times 10^{-12} (T/300)^{-0.7} \text{ cm}^{-3} \text{ mol}^{-1} \text{ s}^{-1}$	Wine et al. <sup>30</sup> Atkinson et al. <sup>31</sup>
R2, $k_2$	$1.3 \times 10^{-12} \exp(-330/T) \text{ cm}^3 \text{ s}^{-1}$	Atkinson et al. <sup>31</sup>
R3, $k_3$	$3.9 \times 10^{-41} \exp(6830.6/T) [\text{H}_2\text{O}]^2 \text{ s}^{-1}$	Jayne et al. <sup>27</sup>
R4, $\sigma_{\text{H}_2\text{O}}$	$7.22 \times 10^{-20} \text{ cm}^2$ (25 °C)	Creasey et al. <sup>29</sup>
R4, $\Phi_{\text{H}_2\text{O}}$	1	Sander et al. <sup>28</sup>
R5, $\sigma_{\text{N}_2\text{O}}$	$1.43 \times 10^{-19} \text{ cm}^2$	Sander et al. <sup>28</sup>
R5, $\Phi_{\text{N}_2\text{O}}$	1	Sander et al. <sup>28</sup>
R6, $k_6$	$2.0 \times 10^{-11} \exp(130/T) \text{ cm}^3 \text{ mol}^{-1} \text{ s}^{-1}$	Atkinson et al. <sup>31</sup>
R7, $k_7$	$7.6 \times 10^{-11} \text{ cm}^3 \text{ mol}^{-1} \text{ s}^{-1}$	Atkinson et al. <sup>31</sup>
R8, $k_8$	$4.3 \times 10^{-11} \text{ cm}^3 \text{ mol}^{-1} \text{ s}^{-1}$	Atkinson et al. <sup>31</sup>
R9, $k_9$	$6.0 \times 10^{-12} \text{ cm}^3 \text{ mol}^{-1} \text{ s}^{-1}$	Atkinson et al. <sup>31</sup>
R10, $k_{10}$	$5.4 \times 10^{-32} (T/300)^{-1.8} [\text{N}_2] \text{ cm}^3 \text{ mol}^{-1} \text{ s}^{-1}$	Atkinson et al. <sup>31</sup>
R11, $k_{11}$	$4.8 \times 10^{-11} \exp(250/T) \text{ cm}^3 \text{ mol}^{-1} \text{ s}^{-1}$	Atkinson et al. <sup>31</sup>
R12, $k_{12}$	$6.9 \times 10^{-31} (T/300)^{-0.8} [\text{N}_2] \text{ cm}^3 \text{ mol}^{-1} \text{ s}^{-1}$	Atkinson et al. <sup>31</sup>
R13, $k_{13}$	$3.6 \times 10^{-12} \exp(270/T) \text{ cm}^3 \text{ mol}^{-1} \text{ s}^{-1}$	Atkinson et al. <sup>31</sup>
$D_{\text{OH}}$	0.215 cm <sup>2</sup> /s	Ivanov et al. <sup>32</sup>
$D_{\text{HO}_2}$	0.141 cm <sup>2</sup> /s	Ivanov et al. <sup>32</sup>
$D_{\text{H}_2\text{SO}_4}$	0.088 cm <sup>2</sup> s <sup>-1</sup> (5% RH, 298 K) to 0.095 cm <sup>2</sup> s <sup>-1</sup> (0% RH, 298 K)	Hanson and Eisele <sup>33</sup>
$D_{\text{SO}_3}$	0.126 cm <sup>2</sup> s <sup>-1</sup> (300 K)	Jayne et al. <sup>27</sup>
$D_{\text{HSO}_3}$	0.126 cm <sup>2</sup> s <sup>-1</sup> (300 K)	same value as for $D_{\text{SO}_3}$

the flow rate ratio between the humidified flow  $Q_{\text{H}_2\text{O}}$  and the total flow through the calibration system:

$$[\text{H}_2\text{O}] = \frac{Q_{\text{H}_2\text{O}}}{Q_{\text{N}_2} + Q_{\text{H}_2\text{O}} + Q_{\text{SO}_2} + Q_{\text{air}}} \cdot \frac{p_{\text{sat}}(T) \cdot N_A}{R \cdot T} \quad (5)$$

This equation assumes that dry nitrogen which is flown through a humidifier (bubbler) becomes saturated with water vapor. The total flow rate consists of the humidified flow ( $Q_{\text{H}_2\text{O}}$ ), SO<sub>2</sub> diluted in nitrogen ( $Q_{\text{SO}_2}$ ), dry air ( $Q_{\text{air}}$ ), and nitrogen ( $Q_{\text{N}_2}$ ). Typical flow rates and concentrations are listed in Table 2. Note that in the reaction scheme R1–R3, the only reaction for the OH radical is the one with SO<sub>2</sub> assuming that other reactions involving OH are negligible. This approximation is made because high-purity gases are used and the concentration of SO<sub>2</sub> is typically ~1 ppmv. Therefore, [SO<sub>2</sub>] is considered to be above the concentrations of potential contaminants in the gas system like CO or hydrocarbons which react with OH as well.

**2.3. Determination of the *It*-Product through N<sub>2</sub>O Actinometry Experiment.** All quantities needed to calculate the amount of produced OH are known except for the *It*-product in eq 4. The two factors of this parameter can either be determined individually<sup>19,20</sup> or they can be determined as their combined product.<sup>21</sup> The first possibility makes use of the absolute photon flux measurement using a calibrated photo diode. However, this method requires a very well-defined illuminated volume and the integration of the photon flux over many points of this volume. In addition, the flow profile needs to be known precisely to calculate the interaction time between

**Table 2.** Gas Flow Rates and Conditions during a Calibration Experiment

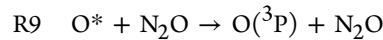
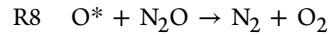
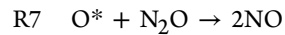
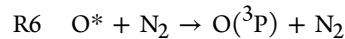
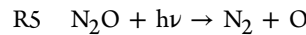
parameter	value	comment
$Q_{\text{SO}_2}$	0.1 slm	SO <sub>2</sub> concentration 100 ppmv in N <sub>2</sub>
$Q_{\text{N}_2}$	10 slm	dilution flow of N <sub>2</sub>
$Q_{\text{air}}$	0.05 slm	synthetic air (21% O <sub>2</sub> and 79% N <sub>2</sub> )
$Q_{\text{H}_2\text{O}}$	0.01 slm to 1.5 slm	N <sub>2</sub> saturated with H <sub>2</sub> O after flowing it through a bubbler
$Q_{\text{total,H}_2\text{SO}_4}$	~10.1 to ~11.6 slm	total flow rate for the H <sub>2</sub> SO <sub>4</sub> experiment
$Q_{\text{CIMS}}$	7.6 slm	CIMS sample flow rate
[SO <sub>2</sub> ]	$\sim 2.5 \times 10^{13} \text{ cm}^{-3}$	concentration of SO <sub>2</sub> in the gas mixture ~1 ppmv
[O <sub>2</sub> ]	$\sim 2.5 \times 10^{16} \text{ cm}^{-3}$	concentration of O <sub>2</sub> in the gas mixture ~1000 ppmv
[H <sub>2</sub> O]	$\sim 5 \times 10^{14} \text{ cm}^{-3}$ to $\sim 5 \times 10^{16} \text{ cm}^{-3}$	water vapor concentration during H <sub>2</sub> SO <sub>4</sub> experiment
[H <sub>2</sub> SO <sub>4</sub> ]	$\sim 5 \times 10^5 \text{ cm}^{-3}$ to $\sim 2 \times 10^9 \text{ cm}^{-3}$	produced [H <sub>2</sub> SO <sub>4</sub> ]
$Q_{\text{N}_2\text{O}}$	<0.3 slm	flow rate of N <sub>2</sub> O during actinometry experiment
$Q_{\text{total,N}_2\text{O}}$	~2 slm	total flow rate during actinometry experiment
$T$	~19 °C	temperature
$L$	25 cm	distance between illuminated region and ion source

UV light and H<sub>2</sub>O for all points. Depending on the setup also the influence of a glass tube which transmits the UV light from an external lamp needs to be taken into account. Therefore, this method includes several experimental challenges and ideally the photo diode needs to be calibrated regularly to account for aging effects.

Due to these challenges we have chosen determining the *It*-product through chemical actinometry. This method makes use of another known chemical reaction which occurs under similar conditions as the actual OH/H<sub>2</sub>SO<sub>4</sub> production experiment. During this separate experiment with a different gas mixture a chemical product is generated through the illumination with UV light at the same intensity as during the H<sub>2</sub>SO<sub>4</sub> experiment. A reaction needs to be chosen for which the rates are known and the reaction products can be measured accurately.

We have chosen the N<sub>2</sub>O to NO<sub>x</sub> conversion for this reference reaction as described by Edwards et al.<sup>21</sup> Earlier studies also made use of an O<sub>2</sub> to O<sub>3</sub> actinometry experiment. However, at 184.9 nm the absorption cross section of oxygen varies strongly for small changes of the wavelength. Since the exact wavelength of the emission line around 184.9 nm for a mercury lamp can vary with temperature very stable and defined conditions are necessary to keep the uncertainty small.<sup>34</sup> Therefore, the N<sub>2</sub>O to NO<sub>x</sub> conversion experiment is preferential.

If only N<sub>2</sub>O and N<sub>2</sub> are present in the flow tube, the following reactions occur:



Solving this reaction scheme yields a relationship between the produced  $\text{NO}_x$  concentration, the concentrations of  $\text{N}_2\text{O}$  and  $\text{N}_2$  as well as the  $It$ -product:

$$It_{\text{N}_2\text{O}} = \frac{k_6 \cdot [\text{N}_2] + (k_7 + k_8 + k_9) \cdot [\text{N}_2\text{O}]}{2 \cdot k_7 \cdot \sigma_{\text{N}_2\text{O}} \cdot \Phi_{\text{N}_2\text{O}} \cdot [\text{N}_2\text{O}]^2} \cdot [\text{NO}_x] \quad (6)$$

The quantum yield for the photolysis of  $\text{N}_2\text{O}$  is unity at 184.9 nm and the absorption cross section is  $1.43 \times 10^{-19} \text{ cm}^2$ .<sup>28</sup> These values as well as the rate constants  $k_6-k_9$  are listed in Table 1. Although only  $\text{N}_2$  and  $\text{N}_2\text{O}$  will be introduced into the calibration system during the actinometry experiment, some oxygen will be produced by reaction R8. This oxygen can react with  $\text{O}(\text{P}^3)$  and produce ozone. Further reaction between ozone and NO produces  $\text{NO}_2$ . Therefore, it is necessary to measure the sum of NO and  $\text{NO}_2$  to derive the  $It$ -product from eq 6 accurately.

Under the same conditions, that is, the flow rates and UV intensities for the  $\text{N}_2\text{O}$  experiment and the  $\text{H}_2\text{SO}_4$  experiment are the same, the effective  $It$ -product will also be identical. Therefore, the UV intensity can be monitored with a suitable photodiode to ensure that the intensity remains constant between the two sets of experiments. However, this photodiode does not need to be calibrated and measure quantitatively, it only needs to monitor that there is no drift in the relative signal, which makes this measurement much easier.

Unfortunately, the concentration of the produced  $\text{NO}_x$  can be quite low (<1 ppbv) and below the detection limit of the  $\text{NO}_x$  monitor. Therefore, it can be necessary to run the  $\text{N}_2\text{O}$  experiment at a lower total flow rate compared to the  $\text{H}_2\text{SO}_4$  experiment (flow rate ~7.6 slm). This way, the effective reaction time within the  $It$ -product changes but because of the linear dependency between the produced  $\text{NO}_x$  and the reaction time the following relationship can be used to relate the two  $It$ -products:

$$It = \frac{Q_{\text{total}, \text{N}_2\text{O}}}{Q_{\text{CIMS}}} \cdot It_{\text{N}_2\text{O}} \quad (7)$$

The validity of this relation over the range of flow rates being used is demonstrated in section 4.1.

**2.4. Model to Calculate Produced  $\text{H}_2\text{SO}_4$  Concentration.** A numerical model has been written which uses a 2d-rotational symmetric geometry (Figure 1 a)). The model

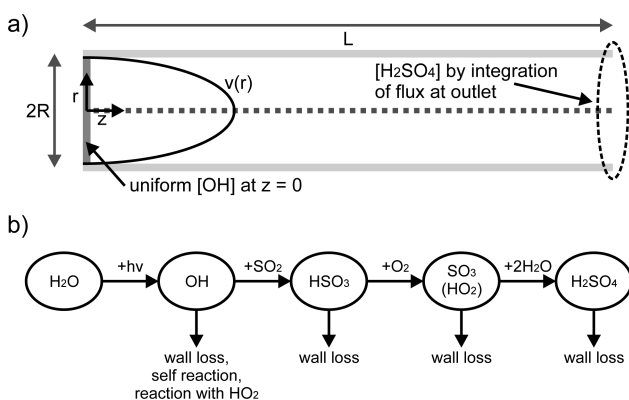
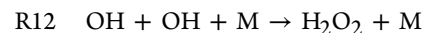
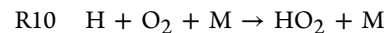


**Figure 1.** a) Model geometry. The actual model makes use of the rotational symmetry and considers only half the geometry shown in the figure (from  $r = 0$  to  $R$ ). b) Reaction scheme for modeling the  $\text{H}_2\text{SO}_4$  production in the calibration system.

calculates the mean sulfuric acid concentration at the end of the 1/2" tube which protrudes into the CIMS ion source.<sup>26</sup> Input parameters are the inner tube diameter ( $D$ ), the length of the tube ( $L$ ), the total flow rate ( $Q_{\text{CIMS}}$ ), the  $It$ -product derived from the  $\text{N}_2\text{O}$  experiment, the gas temperature  $T$  as well as the concentrations of  $\text{SO}_2$ ,  $\text{O}_2$  and  $\text{H}_2\text{O}$ . The main variable is the  $\text{H}_2\text{O}$  concentration because it directly scales the initial OH concentration. The OH is assumed to be homogeneously distributed over the whole cross section of the 1/2" tube at the end of the UV illuminated region (which is approximately 2 cm long). The velocity profile is parabolic which is a reasonable assumption due to a long entrance region (40 cm) and a sufficiently low Reynolds number (~1000 for 7.6 slm total flow rate and an inner tube diameter of 1 cm). In the model, the initial OH concentration according to eq 4 is calculated in the beginning. Starting with the initial gas concentrations, the 2d-time dependent convection diffusion equations for the gas species OH,  $\text{HO}_2$ ,  $\text{SO}_3$ ,  $\text{HSO}_3$ , and  $\text{H}_2\text{SO}_4$  are solved considering the source and sink reactions R1–R3 and the additional reactions R10 to R13 (Table 1 and Figure 1 b)):



The hydrogen atom in R10 originates from the photolysis reaction of  $\text{H}_2\text{O}$  (R4) and reacts rapidly with  $\text{O}_2$  to form  $\text{HO}_2$ . However, the sensitivity of the model to reactions R10 to R12 is very small due to the low concentrations of OH and  $\text{HO}_2$ . These reactions have only been taken into account in order to test the sensitivity of the calibration toward a potential contamination with NO. The abundance of NO would recycle OH and therefore influence the  $\text{H}_2\text{SO}_4$  concentration:



To avoid this effect the calibration system is usually flushed at least for 12 h after a  $\text{N}_2\text{O}$  experiment has been carried out to remove the NO. Additionally, different mass flow controllers are used to control the gas flows during the  $\text{N}_2\text{O}$  and  $\text{H}_2\text{SO}_4$  experiments, respectively. Nevertheless, a sensitivity study with respect to the presence of NO has been carried out to evaluate its potential influence (see section 5).

Over the model domain the concentrations of  $\text{O}_2$ ,  $\text{H}_2\text{O}$  and  $\text{SO}_2$  are assumed to be constant. For the products OH,  $\text{HO}_2$ ,  $\text{SO}_3$ ,  $\text{HSO}_3$  and  $\text{H}_2\text{SO}_4$  wall loss is taken into account. The diffusion coefficients used are listed in Table 1. The following equation is then solved by finite difference method:

$$\frac{\partial c_i[r, z]}{\partial t} = D_i \left( \frac{1}{r} \frac{\partial c_i[r, z]}{\partial r} + \frac{\partial^2 c_i[r, z]}{\partial r^2} + \frac{\partial^2 c_i[r, z]}{\partial z^2} \right) - \left( \frac{2Q}{\pi R^2} \left( 1 - \frac{r^2}{R^2} \right) \right) \cdot \frac{\partial c_i[r, z]}{\partial z} + s_i[r, z] \quad (8)$$

The index  $i$  denotes each of the chemical species (OH,  $\text{HO}_2$ ,  $\text{SO}_3$ ,  $\text{HSO}_3$ , and  $\text{H}_2\text{SO}_4$ ),  $D_i$  the diffusion constants,  $c_i$  the concentrations,  $Q$  the total flow rate (assuming parabolic flow profile), and the term  $s_i$  takes into account the chemical reactions responsible for the production or loss of the respective compound. The set of equations is solved over the whole two-dimensional domain and repeated until a steady

state can be assumed. If this is the case, the flux of  $\text{H}_2\text{SO}_4$  at the tube outlet is integrated over the whole cross sectional area to calculate the mean concentration of sulfuric acid entering the CIMS ion source. This value is assumed to be the true concentration and is used to derive the calibration factor  $C$  from eq 3. The model has been validated with respect to its capability of reproducing diffusional loss of a chemical species with a given diffusion constant. The integrated outward flux of the simulated substance has been compared to the result from a semiempirical equation that is used to calculate diffusion loss and also assumes a fully developed parabolic flow profile.<sup>35</sup> For different flow rates, the discrepancies between both methods are below 1%, indicating that the developed numerical model solves eq 8 with high accuracy. As an example, the transmission of sulfuric acid (for dry conditions, i.e., diffusion coefficient of  $0.095 \text{ cm}^2 \text{ s}^{-1}$ ) through a tube of 25 cm in length is ~67% for a flow rate of 7.6 slm, as used within the calibration system.

### 3. EXPERIMENTAL SECTION

The main part of the calibration source consists of an aluminum box with dimensions of  $30 \times 20 \times 15 \text{ cm}$  ( $L \times W \times H$ ). This box is shown in Figure 2 with its lid removed and is

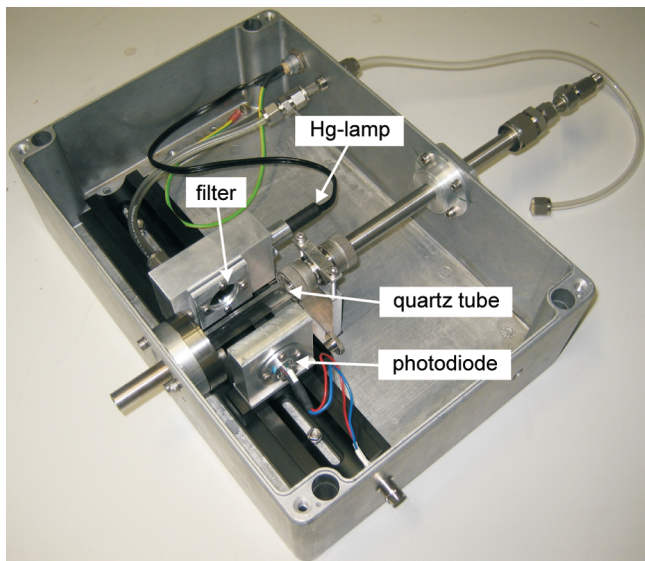


**Figure 2.** Photograph of the calibration box with its lid removed. The dimensions are approximately  $30 \times 20 \times 15 \text{ cm}$ .

similar to the one used by Aufmhoff et al.<sup>20</sup> In Figure 3 a schematic drawing shows the two different configurations for the  $\text{N}_2\text{O}$  and the  $\text{H}_2\text{SO}_4$  experiments used in this study, respectively. The most relevant components housed in this box are highlighted in Figures 2 and 3 and are introduced in the following. Holes have been drilled into the walls of the box, which allow the alignment of a  $1/2"$  tube that goes straight through the box without bends. This is important in order to warrant laminar flow without any development of secondary flows due to wall detachment. Therefore, the transportation and the wall loss of the gas species can be calculated by using a 2d rotationally symmetric geometry. The dimension of the  $1/2"$  tube has been chosen because the CIMS inlet has the same diameter. Therefore, the CIMS can be connected with the calibration box by means of a Swagelok union, which induces only a negligible disturbance to the flow. The tube going through the box consists of three parts; the part in the middle

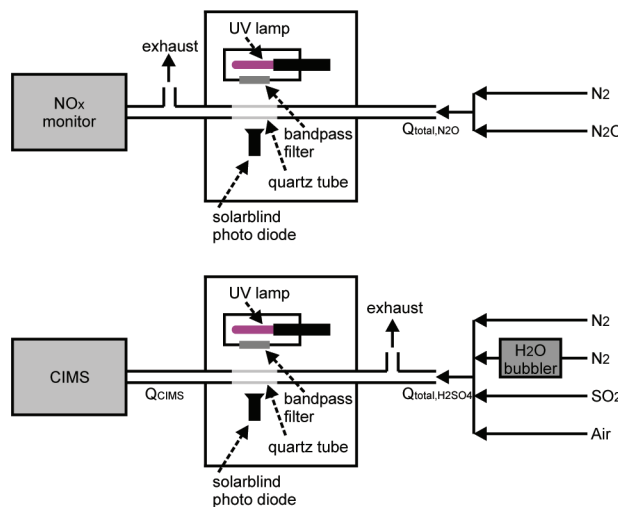


**Figure 3.** Schematic drawing of the calibration unit. Two different configurations are used. The upper one is used to derive the  $I_t$ -product from a  $\text{N}_2\text{O}$  actinometry experiment. The lower one is used to provide stable and known sulfuric acid concentrations for the CIMS. Note that the drawing is not to scale. See text for details.

(~10 cm long) is a  $1/2"$  quartz tube (Suprasil, Aachener Quarzglas Technologie, Germany) that has a high transmission for UV light. This tube is connected to  $1/2"$  stainless steel tubes at both ends. The connections are vacuum-tight through the use of O-ring sealed fittings (Ultratorr, Swagelok, U.S.A.). During a calibration, the box is flushed with dry nitrogen to avoid the absorption of UV light through oxygen and water vapor before it can interact with the gas flowing through the quartz tube. The length of the stainless steel tube that serves as the outlet has been minimized to keep diffusion loss small.

The optical components for illumination of the quartz tube are mounted on an optical rail. A small aluminum block has been machined which houses the mercury lamp (Pen-Ray Lamp 11SC-1, UVP). The UV light emitted from the lamp can leave the aluminum block only through a 20 mm hole which is fully covered by a bandpass filter (UV Bandpass Filter, XB32 185NB20, Horiba). This filter has a high transmission for 185 nm light emitted from the lamp, while the main emission line of the lamp at 254 nm is suppressed. The transmitted light is directed on the center of the quartz tube. This is done by adjusting the vertical position of the lamp such that it corresponds to the center of the bandpass filter and the quartz tube. The horizontal distance between filter and lamp has been minimized to maximize the light intensity penetrating the quartz tube. Directly behind the quartz tube, a solarblind photo diode (Model RS764, Hamamatsu) is aligned on the optical axis. The output of this photo diode is recorded by an electrometer (Model 6514, Keithley). The absolute photo current is, however, not important for the measurements; the photo diode and the electrometer are only needed to monitor the stability and the reproducibility of the UV light intensity. The photon flux is determined by chemical actinometry, as described in sections 2.3 and 3.2.

The calibration box and the UV lamp are continuously flushed with dry nitrogen (between 1 and 2 slm). The nitrogen is introduced into the aluminum block which houses the Hg lamp and leaves it through another small hole. This way, the heat produced by the lamp is transported away as well as any water vapor and oxygen which can absorb the UV light. There

is no temperature sensor installed in the aluminum block yet to monitor the rise in temperature after the lamp has been switched on. Within the first ~30 min after switching on the UV lamp and the gas flow a strong increase in the signal can be seen which is due to the warm-up of the UV lamp, the displacement of the absorbing gases inside the box as well as the temperature change of the lamp and its environment. We usually turn on the gas flows and the UV light at least one hour before an actual calibration measurement is performed. During this time, the photo diode output is monitored and it is ensured that it has reached a stable value.

**3.1. Sulfuric Acid Production Setup.** The configuration of the calibration system used for the production of sulfuric acid is shown in Figure 3. Different mass flow controllers (MFC types 1179B and 1479A, MKS Instruments) are used to provide the flows of dry nitrogen, humidified nitrogen, sulfur dioxide, and dry air. The gases used are of purity 5.0 and their typical flow rates are given in Table 2. The MFCs are calibrated after each experiment against DryCal systems (Definer 220-L/M/H, Bios International Corporation). Nitrogen is humidified by flowing it through a gas wash bottle containing ultrapure water. In order to calculate the water vapor concentration in the gas mixture the exact temperature of the humidified flow needs to be known (eq 5). The temperature is monitored continuously to account for small temperature changes during a calibration with a Pt100 sensor. This method is alternative to controlling the bubbler to a constant temperature. A humidity sensor with high precision and accuracy (type HYT 271, B+B Thermo-Technik GmbH, Germany) has been used to validate that the relative humidity reaches close to 100% within the measurement accuracy of the sensor for all flow rates through the bubbler.

It was also found out that the use of stainless steel tubing instead of using Teflon greatly helps in simplifying the mass spectrum recorded by the CIMS. Berresheim et al.<sup>25</sup> have already shown that a strong signal at  $m/z$  113 ( $\text{CF}_3\text{COO}^-$ ) is present if Teflon (PFA) tubing is used for a gas introduced into the CIMS ion source. For this reason stainless steel was used wherever possible. Only the MFCs (Viton seals) and the o-rings (Viton) are nonstainless steel within the setup. This reduced the signal at  $m/z$  113 substantially although it is still visible in the mass spectrum but its count rate is usually below 1% of the  $m/z$  62 count rate.

The sum of all flow rates ( $Q_{\text{total}, \text{H}_2\text{SO}_4}$ ) is typically around 11 slm. Because the CIMS is only taking 7.6 slm through its inlet ( $Q_{\text{CIMS}}$ ), the difference is vented into an exhaust line before the gases enter the calibration box (Figure 3). The four gas flows are mixed directly behind the MFCs and then flow through a 1/4" tube of about 1 m in length containing many bends to ensure good mixing before the tube expands into a larger diameter in front of the calibration box. The length of this 40 cm long and straight 1/2" diameter tube is sufficient to allow for the development of a laminar flow before the gas reaches the UV illuminated quartz glass section.

**3.2. Setup for  $\text{N}_2\text{O}$  Experiment.** For the determination of the  $It$ -product the configuration described in the previous section is modified slightly. This setup is shown schematically in Figure 3. Instead of the four MFCs providing the  $\text{N}_2$ ,  $\text{SO}_2$ ,  $\text{H}_2\text{O}$ , and zero air, now only flows for  $\text{N}_2\text{O}$  and  $\text{N}_2$  need to be controlled (MFCs type 1179B, MKS Instruments). Ultra-high-purity  $\text{N}_2\text{O}$  (grade 5.0 purity, Messer Griesheim) is used in this configuration. Illuminating the mixture of  $\text{N}_2\text{O}$  and  $\text{N}_2$  with UV light leads to the production of  $\text{NO}_x$  according to section 2.3.

Its concentration is measured with a calibrated commercial  $\text{NO}_x$  monitor (Model APNA-370, Horiba, Ltd.) with a lower detection limit of ~1 ppbv. The sample flow rate of the instrument is approximately 0.8 slm. The  $\text{NO}_x$  monitor is capable of measuring  $\text{NO}_2$  after flowing the sample gas through a molybdenum converter at ~325 °C in which the  $\text{NO}_2$  is reduced to  $\text{NO}$ . This way, the sum of  $\text{NO}$  and  $\text{NO}_2$  is measured. The method for the detection of  $\text{NO}$  relies on chemiluminescence.

Because we wanted to try out different reaction times for the  $\text{N}_2\text{O}$  to  $\text{NO}_x$  conversion (as discussed in section 2.3), the exhaust is moved from the inlet to the outlet of the calibration box. This allows adjusting different flow speeds through the calibration box, while the  $\text{NO}_x$  monitor is operated at its fixed sample flow rate. From the  $\text{N}_2\text{O}$  and  $\text{N}_2$  flow rates, the concentrations for eq 6 can be calculated. The  $It$ -product can be derived by fitting this equation to the measured  $\text{NO}_x$  concentrations. As demonstrated in section 4.1 different flow rates for the separate  $\text{N}_2\text{O}$  and  $\text{H}_2\text{SO}_4$  experiments can be used and the  $It$ -product can be corrected for this difference according to eq 7. Note that the concentration of  $\text{N}_2\text{O}$  that is needed to produce measurable amounts of  $\text{NO}_x$  is typically larger than a few percent of  $\text{N}_2\text{O}$  in  $\text{N}_2$  despite the low flow rate. At this concentration a non-negligible decrease in the measured photo current can be observed due to the absorption of UV light by the  $\text{N}_2\text{O}$ . In contrast, the attenuation during the  $\text{H}_2\text{SO}_4$  experiment is negligible because the  $\text{H}_2\text{O}$  concentration in the total flow is typically below 1%. In addition, the  $\text{H}_2\text{O}$  absorption cross section is about a factor of 2 smaller than for  $\text{N}_2\text{O}$  (Table 1). Since the attenuation in the  $\text{N}_2\text{O}$  experiment can be substantial a correction factor has been derived which takes into account the absorption of UV light (see Appendix A). This correction factor is then used to correct eq 6 for the effect of a nonuniform  $It$ -product.

## 4. RESULTS AND DISCUSSION

### 4.1. $\text{N}_2\text{O}$ to $\text{NO}_x$ Conversion at Different Flow Rates.

First tests with the setup show that only a nonquantifiable amount of  $\text{NO}$  is produced when a total flow rate of 7.6 slm (this corresponds to the CIMS sample flow rate,  $Q_{\text{CIMS}}$ ) is adjusted and the initial volume mixing ratio of  $\text{N}_2\text{O}$  in  $\text{N}_2$  is set to a few percent. For this volume mixing ratio a small increase in the measured  $\text{NO}_x$  concentration could be observed but it did not allow an accurate quantification. Increasing the  $\text{N}_2\text{O}$  concentration would be one possibility for increasing the resulting  $[\text{NO}_x]$ , however, this would lead to a substantial absorption of UV light throughout the 1 cm inner diameter tube and would require a large correction factor to account for this decrease in UV intensity (Appendix A). Therefore, it has been decided to maximize the reaction time for the  $\text{N}_2\text{O}$  to  $\text{NO}_x$  conversion while keeping the  $[\text{N}_2\text{O}]$  as low as possible. To verify that this method can be applied, an experiment with pure  $\text{N}_2\text{O}$  has been performed. The resulting  $\text{NO}_x$  concentration has been recorded as function of the  $\text{N}_2\text{O}$  flow rate. Figure 4 shows the results of this experiment, where  $[\text{NO}_x]$  is plotted against the inverse of the flow rate, which is proportional to the reaction time. The flow rate has been varied between 2 and 10 slm. The line fit through the measured data points indicates a perfect linear relationship between the concentration and the reaction time. This confirms that it is possible to use different flow rates during the  $\text{N}_2\text{O}$  and  $\text{H}_2\text{SO}_4$  experiments and scale the derived  $It$ -product with the flow rate ratio according to eq 7.

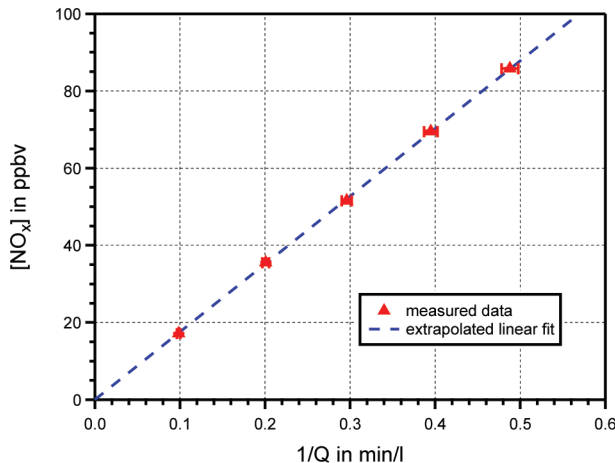


**Figure 4.** Concentration of  $\text{NO}_x$  produced through photolysis of pure  $\text{N}_2\text{O}$  as a function of the reaction time. Because the exact reaction time is not known, the inverse of the flow rate is used. See text for details.

#### 4.2. Measurement of the $It$ -Product through Chemical Actinometry.

Figure 5 shows the measured  $\text{NO}_x$  concen-

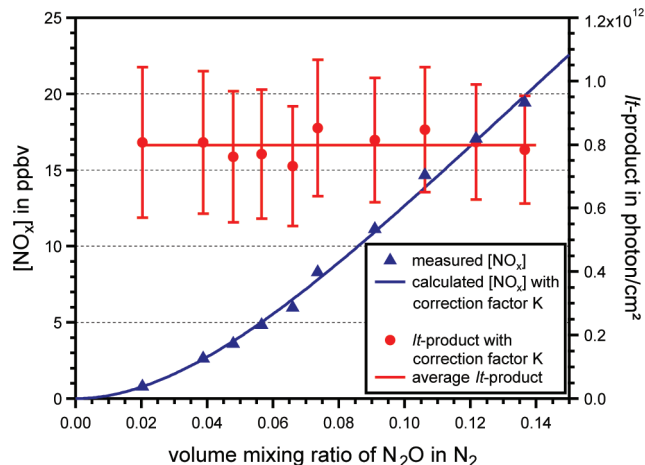


**Figure 5.** Produced amount of  $\text{NO}_x$  during the  $\text{N}_2\text{O}$  actinometry experiment. The average value of the derived  $It$ -product is  $7.98 \times 10^{11}$   $\text{photon cm}^{-2}$  (for a flow rate of  $Q_{\text{CIMS}} = 7.6$  slm).

trations for different  $\text{N}_2\text{O}$  volume mixing ratios. Despite the relatively low mixing ratios used, the absorption of UV light is non-negligible for most of the data points shown in Figure 5. Therefore, a geometry-dependent correction factor  $K$  has been calculated for each data point (see Appendix A). This correction factor takes into account the attenuation of the UV light along its path through the quartz tube. With this factor it is possible to derive a representative value for the  $It$ -product also for higher  $\text{N}_2\text{O}$  mixing ratios. The  $It$ -product values shown in Figure 5 have been scaled according to the different flow rate which was used during the  $\text{N}_2\text{O}$  actinometry experiment ( $\sim 2$  slm) as compared to the 7.6 slm used for the  $\text{H}_2\text{SO}_4$  experiment. As can be seen from the small scatter in the data points the value can be derived with high precision when using the geometry dependent correction factor  $K$ . This demonstrates the importance of considering the UV light attenuation. The value of the  $It$ -product derived from this experiment is  $7.98 \times 10^{11}$   $\text{photon cm}^{-2}$ .

Because deriving the  $It$ -product is the key part of the calibration method, further discussion about its accuracy follows. The  $\text{NO}_x$ -monitor is calibrated with gas standards diluted in pure nitrogen prior to an experiment. During the actual  $\text{N}_2\text{O}$  experiment, however, a substantial concentration of  $\text{N}_2\text{O}$  is present (up to  $\sim 10\%$  of the total flow). Since  $\text{N}_2\text{O}$  is more efficient than  $\text{N}_2$  in terms of quenching excited  $\text{NO}_2^*$  molecules, which irradiate the light used for measuring  $\text{NO}$ , this effect needs to be investigated. Therefore, another measurement was performed where different mixing ratios of  $\text{N}_2\text{O}$  were added to a  $\text{NO}$  gas standard diluted with nitrogen to test by how much the detected  $\text{NO}$  concentration drops due to the quenching of  $\text{NO}_2^*$  by  $\text{N}_2\text{O}$ . At a mixing ratio of 0.1 for  $\text{N}_2\text{O}$  and a nominal  $\text{NO}$  concentration of 10 ppbv, the reduction in detection efficiency is somewhat smaller than 5% due to the presence of  $\text{N}_2\text{O}$ . For lower concentrations of  $\text{N}_2\text{O}$  and  $\text{NO}$ , respectively, the deviation was even lower. Therefore, the quenching can be non-negligible for high concentrations of  $\text{N}_2\text{O}$ ; however, for this study, its effect seems to be small. In addition, the effect is not constant for all data points shown and can lead to a maximum deviation of 5% only for the data points at high  $[\text{N}_2\text{O}]$ . This can then shift the fitted  $It$ -product to slightly higher values. The exact quantification of this effect is challenging because it would require the accurate determination of very small differences in the detection efficiency of  $\text{NO}_x$  for all data points in Figure 5 due to the varying concentrations of  $\text{N}_2\text{O}$  and  $\text{NO}$ . Therefore, in this case, only the maximum possible deviation is stated in Table 3 which can be up to 5%

**Table 3. Uncertainties of the Relevant Parameters for the Calibration System<sup>a</sup>**

parameter	value or uncertainty
$T$	$\pm 1^\circ\text{C}$
$It$	$7.98 \times 10^{11}$ $\text{photon cm}^{-2}$ statistical error: $0.12 \times 10^{11}$ (1.5%) systematic error: $2.39 \times 10^{11}$ (30%)*
$\sigma_{\text{N}_2\text{O}}$	2%
$\Phi_{\text{N}_2\text{O}}$	1%
$k_6 - k_9$	10%
$[\text{N}_2\text{O}]$	overall error: 5%
$[\text{NO}_x]$	overall error: 5%
$[\text{H}_2\text{O}]$	overall error: 10% (mainly based on $\Delta T$ )
$L$	4%
$Q_{\text{CIMS}}$	5%
$C$	$1.099 \times 10^{10}$ $\text{cm}^{-3}$ statistical error $3.2 \times 10^8$ $\text{cm}^{-3}$ (2.9%) systematic error $3.6 \times 10^9$ $\text{cm}^{-3}$ (33%)*

\*Please note that the effect of  $\text{N}_2\text{O}$  on the detection efficiency of the  $\text{NO}_x$ -monitor is not included here. This effect is in any case smaller than 5% with respect to  $It$  and  $C$  (see discussion in section 4.2).

but is probably smaller because only the points for the high  $\text{NO}_x$  concentrations in Figure 5 are affected.

**4.3. Calibration Factor for Different  $\text{H}_2\text{SO}_4$  Concentrations.** Figure 6 shows the data from a  $\text{H}_2\text{SO}_4$  calibration experiment. The gas flows during this calibration had been adjusted according to the values given in Table 2. Before 13:00, no water vapor was introduced into the calibration system. The signal obtained during this period is considered as the background signal originating from instrumental noise as well as from a small cross-sensitivity to  $\text{SO}_2$ .<sup>26</sup> In addition, even when no water vapor is actively introduced into the calibration system its concentration is not zero since there is always some water evaporating from the stainless steel tubing. This

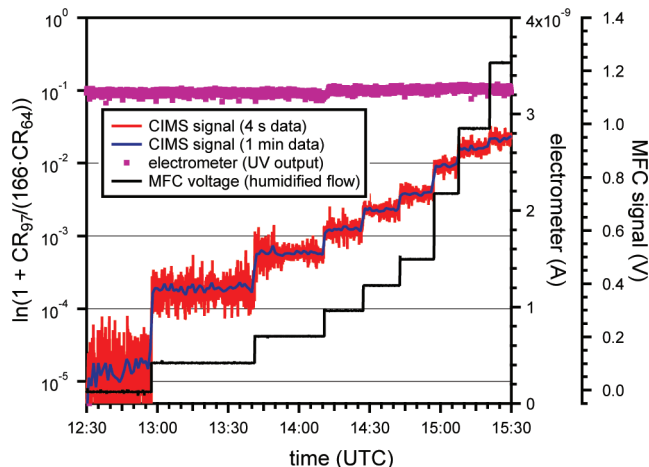


**Figure 6.** Time series showing the different steps of the calibration procedure.

contribution can be minimized by flushing the system with dry nitrogen over a long time and heating it. Nevertheless, a slight increase in the signal is always observed when the UV light is turned on (if  $\text{SO}_2$  is present) even without adding water vapor. However, this effect can be accounted for by subtracting the offset value from the signals when water vapor is added.

At  $\sim 13:00$ , the MFC controlling the flow through the water bubbler was turned on which resulted in the production of sulfuric acid. The flow through the bubbler was then increased after a certain time in order to step through different  $\text{H}_2\text{O}$  concentrations while leaving all other parameters constant. In Figure 6, also the photodiode signal recorded by the electrometer is shown. The measurement shows that the intensity was constant during the whole course of the experiment.

For the conditions during the calibration shown in Figure 6 the sulfuric acid concentration has been calculated with the model described in section 2.4. An  $I\tau$ -product of  $7.98 \times 10^{11}$  photon  $\text{cm}^{-2}$  as derived from the  $\text{N}_2\text{O}$  experiment described in section 4.2 has been used. The calculated  $\text{H}_2\text{SO}_4$  concentrations are shown in Figure 7 as a function of the water vapor concentration in the calibration gas. The  $\text{SO}_3$  concentrations at the outlet have been calculated as well and are plotted in the same figure. It can be seen that for the low water vapor concentrations ( $\sim < 5 \times 10^{15}$  molecules  $\text{cm}^{-3}$ ) the  $\text{SO}_3$  is inefficiently converted to  $\text{H}_2\text{SO}_4$ . Therefore, for the low humidities, the rate limiting step in the  $\text{H}_2\text{SO}_4$  production is not defined by reaction R1 but by reaction R3. This is an important feature of our calibration system and will be discussed further below.

From the measured quantity  $\ln(1 + CR_{97}/(166 \cdot CR_{64}))$  averaged over each step of a constant water vapor concentration and the respective calculated  $\text{H}_2\text{SO}_4$  concentration a calibration factor is obtained according to eq 3. The result is shown in Figure 8, where the factor  $C$  is plotted against the calculated sulfuric acid concentration. It has a constant value with small scatter for  $[\text{H}_2\text{SO}_4] > 3 \times 10^7$  molecules  $\text{cm}^{-3}$ . The average value of  $C$  for this regime is  $1.099 \times 10^{10}$   $\text{cm}^{-3}$ . For lower concentrations the factor decreases and for  $[\text{H}_2\text{SO}_4] = 5 \times 10^5$  molecules  $\text{cm}^{-3}$  it reaches  $\sim 27\%$  of the average value obtained for the high sulfuric acid concentrations. This would mean that the efficiency for detecting sulfuric acid is higher at low concentrations; something that contradicts the assumption

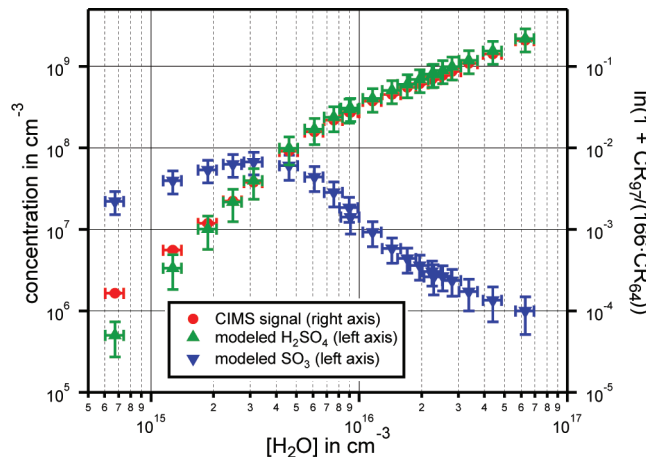


**Figure 7.** Modeled concentrations of  $\text{H}_2\text{SO}_4$  and  $\text{SO}_3$  as function of water vapor concentration in the calibration system. Note that the axis on the right-hand side is not showing  $[\text{H}_2\text{SO}_4]$  but the signals recorded by the CIMS which are a measure for the sulfuric acid concentration. This signal is then used to derive the calibration factor (see text for details and also Figure 8).

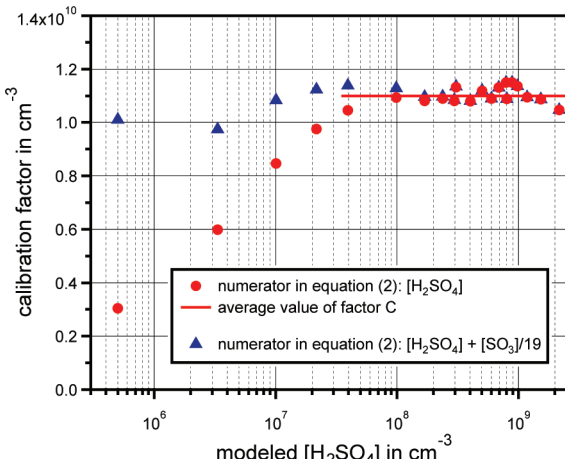


**Figure 8.** Calibration factor for different  $\text{H}_2\text{SO}_4$  concentrations. The average value highlighted by the horizontal bar is  $1.099 \times 10^{10} \text{ cm}^{-3}$ .

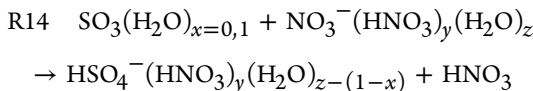
that CIMS has a linear response over a wide range of concentrations and one constant calibration factor can be used. Whether this can indeed be the case is discussed in the following section.

## 5. DISCUSSION

It is an important question whether the decreasing value of the calibration factor in Figure 8 is real or due to limitations in the model which calculates the  $\text{H}_2\text{SO}_4$  concentrations.

We propose that it is more likely that the model is causing the concentration dependent value due to one or more unknown reactions which are most efficient when the concentrations of  $\text{H}_2\text{O}$  are low. One candidate compound could be the  $\text{SO}_3$  which has only high concentrations at low water vapor (and low  $\text{H}_2\text{SO}_4$ ) concentrations. The presence of this compound is confirmed for low water concentrations through the observation of characteristic ion signals obtained during mass scans (discussed further below). When the  $\text{SO}_3$  enters the CIMS ion source collisions with  $\text{NO}_3^-$  ions take

place. Since the  $\text{NO}_3^-$  ions will be bound to nitric acid as well as water molecules, the following reaction could occur:<sup>36</sup>



This reaction would lead to the detection of  $\text{HSO}_4^-$  because the collision dissociation chamber in the CIMS instrument would strip off most of the nitric acid and water from the core ions. The measurement cannot discriminate by which reaction (either from  $\text{SO}_3$  or  $\text{H}_2\text{SO}_4$ ) the  $\text{HSO}_4^-$  has been created from. If some detected  $\text{HSO}_4^-$  originates from reaction R14, the measured  $[\text{H}_2\text{SO}_4]$  would be overestimated. This would result in a smaller calibration factor  $C$  for the cases where the relative amount of  $\text{SO}_3$  is high compared to  $\text{H}_2\text{SO}_4$ . To test this hypothesis, some fraction (about 5%) of the  $[\text{SO}_3]$  has been added to the modeled sulfuric acid concentrations and the calibration factor has been recalculated (Figure 8). This assumption indeed results in a much more constant calibration factor by affecting only the values for the low sulfuric acid concentrations and not the ones for the higher concentrations.

The attempt to quantify the contribution from  $\text{SO}_3$  to the sulfuric acid based on measurements has not been made, although ion signals resulting from  $\text{SO}_3$  have been observed during mass scans performed during a calibration experiment. These signals show up at  $m/z$  96 ( $\text{SO}_4^-$  ion from reaction of  $\text{SO}_3$  and  $\text{NO}_3^-$ ) as well as at  $m/z$  142 ( $\text{SO}_4^-(\text{NO}_2)$  ion from reaction of  $\text{SO}_3$  and  $\text{NO}_3^-(\text{HNO}_3)$ ), respectively.<sup>37</sup> The signals at these  $m/z$  values were, however, only be pronounced when the  $\text{H}_2\text{O}$  concentrations were rather low ( $\sim 10^{15} \text{ cm}^{-3}$ ), thereby confirming the results from modeling the  $\text{SO}_3$  concentration (Figure 7). Translating the observed  $\text{SO}_3$  signals into an effective contribution to the measured sulfuric acid concentration is, unfortunately, not possible. For this, the concentrations of the compounds in reaction R14 would be required together with the reaction rates; all of which are, however, unknown. Nevertheless, the observation of  $\text{SO}_3$  indicates that reaction R14 could be occurring.

Another interference that could affect the sulfuric acid concentration for a given OH concentration could arise from contamination of the calibration gases with  $\text{NH}_3$ .<sup>38</sup> Such a contamination cannot be ruled out if considered that even under the extremely clean conditions of the CLOUD experiment a contamination with  $\text{NH}_3$  (<35 pptv) occurred.<sup>8</sup> If  $\text{NH}_3$  was present in our system it competes with  $\text{H}_2\text{O}$  for the reaction with  $\text{SO}_3$ . Taking into account the rates for the  $\text{SO}_3$  and  $\text{NH}_3$  reaction as well as for the  $\text{SO}_3$  and  $\text{H}_2\text{O}$  reaction (from Lovejoy et al.<sup>39</sup> and Jayne et al.<sup>27</sup>), it can be estimated that for  $[\text{NH}_3] = 250 \text{ pptv}$  both reactions would occur at the same rate (for  $[\text{H}_2\text{O}] = 10^{15} \text{ cm}^{-3}$ ). It should, however, be noted that if this parallel reaction with ammonia occurs it would move the data points for the low water vapor concentrations in Figure 8 above the highlighted number of the calibration factor. This would therefore be the opposite effect as what the observation is showing. In addition, for higher water concentrations the effect of competing reactions would become smaller or require even much higher contaminant levels which can most likely be ruled out.

Due to these considerations we assume that the value of  $C = 1.1 \times 10^{10} \text{ molecules cm}^{-3}$  is valid over the whole range of  $[\text{H}_2\text{SO}_4]$  from  $5 \times 10^5$  to  $2 \times 10^9 \text{ molecules cm}^{-3}$  tested. This value is within the range of  $4.7 \times 10^9$  and  $1.89 \times 10^{10} \text{ molecules cm}^{-3}$  which has been reported by other authors using similar CIMS instruments.<sup>40–43</sup> Most of these studies did not report the exact conditions under which the calibrations were performed and whether their calibration factor was derived under systematically varied conditions. The only study we are aware of which has validated the calibration factor for  $\text{HO}_x$  measurements over a wider range of concentrations is the one by Kukui et al.<sup>23</sup> While they were using a similar calibration technique, they did not see any dependence on the nominal concentration. However, the relative humidity in their system was larger than 2.2% ( $= 1.3 \times 10^{16} \text{ molecules cm}^{-3}$  assuming  $T = 293.15 \text{ K}$ ) and therefore probably high enough to ensure the complete conversion of  $\text{SO}_3$  to  $\text{H}_2\text{SO}_4$ .

It is also worth comparing the effective reaction time derived from the calibration factor to the value, which can be derived from the CIMS ion source geometry and the flow rate. When a reaction rate of  $k = 1.87 \times 10^{-9} \text{ cm}^3 \text{ s}^{-1}$  is used ( $\text{H}_2\text{SO}_4$  and  $\text{NO}_3^-(\text{HNO}_3)$  reaction<sup>17</sup>), the effective reaction time can be evaluated as 0.049 s from the calibration. In comparison, the dwell time of sulfuric acid in the ion source (based on plug flow) is 0.142 s. This large difference shows that a calibration of the CIMS is imperative if accurate measurements need to be made. What causes this large discrepancy is subject to future work; possible sources of error are the value of the reaction rate, the assumption of plug flow, and whether the  $\text{NO}_3^-$  ions mix instantaneously with the sulfuric acid as soon as it enters the ion source.

Table 3 summarizes the uncertainties of the parameters relevant to the calibration system. The accuracy of the calibration factor  $C$  is 33%. This uncertainty originates mainly from the determination of the  $It$ -product value. It should be noted, however, that the rate constant for R1 is only reliable within a factor of 2.<sup>31</sup> This effect would influence the accuracy of the calibration factor only slightly if no other competing reactions are occurring. Therefore, this uncertainty has not been included in the error calculation shown in Table 3.

The sensitivity of the model has been tested toward NO contamination because NO can recycle OH through its reaction with  $\text{HO}_2$ . During the  $\text{N}_2\text{O}$  actinometry experiments, NO is produced, however, the lines are thoroughly flushed afterward and no NO is measurable once the UV light is off. Nevertheless, assuming a contamination of 5 ppbv (which is considerably above the detection limit of the  $\text{NO}_x$ -monitor) the influence on the modeled  $[\text{H}_2\text{SO}_4]$  was <2% for all conditions and can therefore be neglected.

## 6. SUMMARY AND CONCLUSIONS

A calibration system for a chemical ionization mass spectrometer (CIMS) measuring gaseous sulfuric acid has been set up and characterized. This system consists of a box containing a UV lamp, a bandpass filter to provide mainly 185 nm light from a UV lamp, a quartz glass tube and a solarblind photodiode. Several mass flow controllers provide flows of  $\text{SO}_2$ , air and  $\text{N}_2$  into the quartz tube. During a calibration different water vapor concentrations are added to the gas mixture which results in different  $\text{H}_2\text{SO}_4$  concentrations initiated by the photolysis of  $\text{H}_2\text{O}$  which produces OH. A numeric model has been written which calculates the concentration of sulfuric acid that will be available at the outlet of the calibration box. The  $It$ -product (product of photon flux at 185 nm and illumination time) for calculating the  $[\text{H}_2\text{SO}_4]$  is derived from separate chemical actinometry experiments using  $\text{N}_2\text{O}$  to  $\text{NO}_x$  conversion. From the calculated  $\text{H}_2\text{SO}_4$  and the ion signal

measured by CIMS a calibration factor can be derived. This factor  $C$  has a value of  $1.1 \times 10^{10}$  molecules  $\text{cm}^{-3}$ , which agrees well with literature data. However, it was found that the calibration factor is biased to lower values for lower nominal  $\text{H}_2\text{SO}_4$  concentrations produced by the calibration system. It is suspected that this deviation is due to the low water vapor concentrations present at these conditions. At low  $[\text{H}_2\text{O}]$  the conversion of  $\text{SO}_3$  to  $\text{H}_2\text{SO}_4$  does not occur fast enough and therefore  $\text{SO}_3$  will be introduced into the CIMS. We speculate that a part of this  $\text{SO}_3$  is detected as  $\text{HSO}_4^-$  through ion molecule reaction with  $\text{NO}_3^-(\text{HNO}_3)_y(\text{H}_2\text{O})_z$ . This is supported by the fact that ion signals from  $\text{SO}_3$  were observed for low water vapor concentrations. So far we have not tried to quantify the  $[\text{SO}_3]$  coming from our calibration system. Lovejoy et al.<sup>39</sup> have reported that the relative detection sensitivity ( $\text{H}_2\text{SO}_4/\text{SO}_3$ ) is approximately 3.1, which would need to be verified.

In the future we plan to investigate the potential influence of reaction R14 on our calibration system. This could be done, for example, by inserting a porous tube saturated with water in between the calibration box and the CIMS. The OH production would then be decoupled from the further reactions leading to the generation of sulfuric acid without being limited by the abundance of water vapor. Therefore, all  $\text{SO}_3$  should be converted to  $\text{H}_2\text{SO}_4$  before the gas enters the CIMS ion source.

If a concentration-dependent calibration factor can occur in other calibration systems as well depends on the conditions used but it could in principle be the case when reaction times are short and water vapor concentrations are low (as discussed also by Mauldin et al.<sup>41</sup>). Whether this is the case can be checked by varying the nominal sulfuric acid concentration from such systems over a wide range. Various groups are measuring the concentration of sulfuric acid by CIMS methods relying on similar types of calibrations. The calibration system introduced in this study can be used to intercompare different CIMS instruments under defined conditions.

## APPENDIX A

Deriving the  $It$ -product from the  $\text{N}_2\text{O}$  actinometry experiment requires taking into account the attenuation of UV light traversing through the quartz glass tube. In this section an expression for the relationship between the effective  $It$ -product, the measured  $\text{NO}_x$  concentration, the geometry, and the initial  $\text{N}_2\text{O}$  concentration is derived. The assumption is made that the UV light traversing the tube is parallel, perpendicular to the direction of flow inside the tube and parallel to the optical axis defined by the detector, the tube, the bandpass filter, and the lamp. Figure 9 shows the geometry that is used to describe the

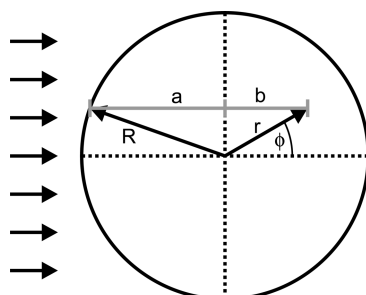


**Figure 9.** Geometry for deriving the correction factor  $K$ . Direction of flow is perpendicular to the page.

photon intensity in cylinder coordinates  $(r, \varphi)$ . Using the nomenclature in the figure the  $It$ -product can be described as a function of  $r$  and  $\varphi$  as follows:

$$It(r, \varphi) = I_0 \cdot \exp(-\sigma_{\text{N}_2\text{O}} \cdot [\text{N}_2\text{O}] \cdot (a + b)) \cdot t_r(r) \quad (\text{A1})$$

where the reaction time  $t_r$  is dependent on the radial position due to the parabolic velocity profile of the flow. This formulation makes use of the Lambert–Beer law where the absorption path length is the sum of the distances  $a$  and  $b$ :

$$a = (R^2 - (r \cdot \sin \varphi)^2)^{0.5} \quad b = r \cdot \cos \varphi \quad (\text{A2})$$

The measurable  $\text{NO}_x$  concentration that is produced in the quartz tube is

$$[\text{NO}_x] = \frac{2 \int_{r=0}^R \int_{\varphi=0}^{\pi} v(r) \cdot [\text{NO}_x](r, \varphi) \cdot r \cdot d\varphi \cdot dr}{v_{\text{avg}} \cdot \pi \cdot R^2} \quad (\text{A3})$$

Here, the  $\text{NO}_x$  concentration which is produced at any given point in the tube is a function of  $r$  and  $\varphi$  as well. Weighting this concentration with the flow speed  $v$  and integrating over the whole cross-sectional area results in the effective mean  $\text{NO}_x$  concentration.

When eq 6 is used and considering the dependency of  $It$  on  $r$  and  $\varphi$ , the local  $\text{NO}_x$  concentration can be expressed as

$$[\text{NO}_x](r, \varphi) = \frac{2 \cdot k_7 \cdot \sigma_{\text{N}_2\text{O}} \cdot \Phi_{\text{N}_2\text{O}} \cdot [\text{N}_2\text{O}]^2}{k_6 \cdot [\text{N}_2] + (k_7 + k_8 + k_9) \cdot [\text{N}_2\text{O}]} \cdot It(r, \varphi) \quad (\text{A4})$$

Inserting this relationship into eq A3 and using

$$t_r(r) = \frac{L_r}{v(r)} \quad (\text{A5})$$

with the effective length  $L_r$  over which the gas is illuminated with UV light, yields

$$[\text{NO}_x] = \frac{2 \cdot k_7 \cdot \sigma_{\text{N}_2\text{O}} \cdot \Phi_{\text{N}_2\text{O}} \cdot [\text{N}_2\text{O}]^2}{k_6 \cdot [\text{N}_2] + (k_7 + k_8 + k_9) \cdot [\text{N}_2\text{O}]} \cdot \frac{I_0 \cdot L_r}{v_{\text{avg}}} \cdot K \quad (\text{A6})$$

The geometry factor  $K$  is defined as

$$K = \frac{2 \int_{r=0}^R \int_{\varphi=0}^{\pi} \exp(-\sigma_{\text{N}_2\text{O}} \cdot [\text{N}_2\text{O}] \cdot (a + b)) \cdot r \cdot d\varphi \cdot dr}{\pi \cdot R^2} \quad (\text{A7})$$

Reformulating and identifying  $L_r/v_{\text{avg}}$  as the mean reaction time  $t_r$  yields:

$$I \cdot t_r = \frac{k_6 \cdot [\text{N}_2] + (k_7 + k_8 + k_9) \cdot [\text{N}_2\text{O}]}{2 \cdot k_7 \cdot \sigma_{\text{N}_2\text{O}} \cdot \Phi_{\text{N}_2\text{O}} \cdot [\text{N}_2\text{O}]^2} \cdot \frac{[\text{NO}_x]}{K} \quad (\text{A8})$$

Finally, this equation can be used to evaluate the effective  $It$ -product for the different flow rate of the  $\text{H}_2\text{SO}_4$  experiment:

$$It = \frac{k_6 \cdot [\text{N}_2] + (k_7 + k_8 + k_9) \cdot [\text{N}_2\text{O}]}{2 \cdot k_7 \cdot \sigma_{\text{N}_2\text{O}} \cdot \Phi_{\text{N}_2\text{O}} \cdot [\text{N}_2\text{O}]^2} \cdot \frac{[\text{NO}_x]}{K} \cdot \frac{Q_{\text{total}, \text{N}_2\text{O}}}{Q_{\text{CIMS}}} \quad (\text{A9})$$

This shows that instead of using a constant photon flux over the whole cross-sectional area the geometry factor  $K$  needs to be calculated which depends on the  $\text{N}_2\text{O}$  concentration and its absorption cross-section as well as on the tube radius. For negligible absorption this factor approaches a value of 1. The evaluation of the actual values of  $K$  is done by integrating eq A7 numerically. For the geometry used here and the  $\text{N}_2\text{O}$  concentrations in Figure 5  $K$  varies between 0.97 (at a  $\text{N}_2\text{O}$  volume mixing ratio of 0.02) and 0.82 (at a  $\text{N}_2\text{O}$  volume mixing ratio of 0.14). Therefore, only for the very low mixing ratios the UV attenuation can be neglected. However, the  $It$ -product from these lower values can only be determined with higher uncertainty because of the low amount of  $\text{NO}_x$  produced. Therefore, the correction is required because it allows taking into account also  $It$ -values derived from higher concentrations of  $\text{N}_2\text{O}$  and  $\text{NO}_x$  with a higher signal-to-noise ratio.

## AUTHOR INFORMATION

### Corresponding Author

\*Phone: +49 (0)69 798 40256. Fax: +49 (0)69 798 40262. E-mail: kuerten@iau.uni-frankfurt.de.

### Notes

The authors declare no competing financial interest.

## ACKNOWLEDGMENTS

We thank D. J. Tanner, L. G. Huey, and R. Stickel from THS Instruments for helpful discussions and technical support. The research leading to these results has received funding from the EC's Seventh Framework Programme under Grant Agreement No. 215072 (Marie Curie Initial Training Network "CLOUD-ITN") and from the German Federal Ministry of Education and Research (Project No. 01LK0902A "CLOUD-09").

## REFERENCES

- (1) Kulmala, M.; Vehkämäki, H.; Petäjä, T.; Dal Maso, M.; Lauri, A.; Kerminen, V.-M.; Birmili, W.; McMurry, P. H. *J. Aerosol Sci.* **2004**, *35*, 143–176.
- (2) IPCC. Climate Change 2007: the Physical Science Basis. Contribution of Working Group I to the Fourth Assessment Report of the Intergovernmental Panel on Climate Change, Cambridge University Press: Cambridge, U.K., 2007.
- (3) Merikanto, J.; Spracklen, D. V.; Mann, G. W.; Pickering, S. J.; Carslaw, K. S. *Atmos. Chem. Phys.* **2009**, *9*, 8601–8616.
- (4) Weber, R. J.; McMurry, P. H.; Eisele, F. L.; Tanner, D. J. *J. Atmos. Sci.* **1995**, *52*, 2242–2257.
- (5) Fiedler, V.; Dal Maso, M.; Boy, M.; Aufmhoff, H.; Hoffmann, J.; Schuck, T.; Birmili, W.; Hanke, M.; Uecker, J.; Arnold, F.; et al. *Atmos. Chem. Phys.* **2005**, *5*, 1773–1785.
- (6) Kuang, C.; McMurry, P. H.; McCormick, A. V.; Eisele, F. L. *J. Geophys. Res.* **2008**, *113*, D10209.
- (7) Laaksonen, A.; Kulmala, M.; Berndt, T.; Stratmann, F.; Mikkonen, S.; Ruuskanen, A.; Lehtinen, K. E. J.; Dal Maso, M.; Aalto, P.; Petäjä, T.; et al. *Atmos. Chem. Phys.* **2008**, *8*, 7255.
- (8) Kirkby, J.; Curtius, J.; Almeida, J.; Dunne, E.; Duplissy, J.; Ehrhart, S.; Franchin, A.; Gagné, S.; Ickes, L.; Kürten, A.; et al. *Nature* **2011**, *476*, 429–435.
- (9) Ball, S. M.; Hanson, D. R.; Eisele, F. L.; McMurry, P. H. *J. Geophys. Res. Atmos.* **1999**, *104*, 23709–23718.
- (10) Zhang, R. Y.; Suh, I.; Zhao, J.; Zhang, D.; Fortner, E. C.; Tie, X. X.; Molina, L. T.; Molina, M. J. *Science* **2004**, *304*, 1487–1490.
- (11) Metzger, A.; Verheggen, B.; Dommen, J.; Duplissy, J.; Prevot, A. S. H.; Weingartner, E.; Riipinen, I.; Kulmala, M.; Spracklen, D. V.; Carslaw, K. S.; et al. *Proc. Natl. Acad. Sci. U.S.A.* **2010**, *6646*–6651.
- (12) Berndt, T.; Stratmann, F.; Sipilä, M.; Vanhanen, J.; Petäjä, T.; Mikkilä, J.; Gruner, A.; Spindler, G.; Mauldin, R. L. III; Curtius, J.; et al. *J. Atmos. Chem. Phys.* **2010**, *10*, 7101–7116.
- (13) Hanson, D. R.; Lovejoy, E. R. *J. Phys. Chem. A* **2006**, *110*, 9525–9528.
- (14) Petäjä, T.; Sipilä, M.; Paasonen, P.; Nieminen, T.; Kurtén, T.; Ortega, I. K.; Stratmann, F.; Vehkämäki, H.; Berndt, T.; Kulmala, M. *Phys. Rev. Lett.* **2011**, *106*, 228302–1–228302–4.
- (15) Kupc, A.; Amorim, A.; Curtius, J.; Danielczok, A.; Duplissy, J.; Ehrhart, S.; Walther, H.; Ickes, L.; Kirkby, J.; Kürten, A.; et al. *J. Aerosol Sci.* **2011**, *42*, 532–543.
- (16) Voigtländer, J.; Duplissy, J.; Stratmann, F. *Atmos. Chem. Phys. Discuss.* **2011**, *11*, 20013–20049.
- (17) Viggiano, A. A.; Seeley, J. V.; Mundis, P. L.; Williamson, J. S.; Morris, R. A. *J. Chem. Phys. A* **1997**, *101*, 8275–8278.
- (18) Dusanter, S.; Vimal, D.; Stevens, P. S. *Atmos. Chem. Phys.* **2008**, *8*, 321–340.
- (19) Young, L. H.; Benson, D. R.; Kameel, F. R.; Pierce, J. R.; Junninen, H.; Kulmala, M.; Lee, S.-H. *Atmos. Chem. Phys.* **2008**, *8*, 4997–5016.
- (20) Aufmhoff, H.; Hanke, M.; Uecker, J.; Schlager, H.; Arnold, F. *Int. J. Mass Spectrom.* **2011**, *308*, 26–34.
- (21) Edwards, G. D.; Cantrell, C. A.; Stephens, S.; Hill, B.; Goyea, O.; Shetter, R. E.; Mauldin, R. L. III; Kosciuch, E.; Tanner, D. J.; Eisele, F. L. *Anal. Chem.* **2003**, *75*, 5317–5327.
- (22) Faloon, I. C.; Tan, D.; Lesher, R. L.; Hazen, N. L.; Frame, C. L.; Simpas, J. B.; Harder, H.; Martinez, M.; Di Carlos, P.; Ren, X.; et al. *J. Atmos. Chem.* **2004**, *47*, 139–167.
- (23) Kukui, A.; Ancellet, G.; Le Bras, G. *J. Atmos. Chem.* **2008**, *61*, 133–154.
- (24) Eisele, F. L.; Tanner, D. J. *J. Geophys. Res.* **1993**, *98*, 9001–9010.
- (25) Berresheim, H.; Elste, T.; Plass-Dülmer, C.; Eisele, F. L.; Tanner, D. J. *Int. J. Mass Spectrom.* **2000**, *202*, 91–109.
- (26) Kürten, A.; Rondo, L.; Ehrhart, S.; Curtius, J. *Atmos. Meas. Technol.* **2011**, *4*, 437–443.
- (27) Jayne, J. T.; Pöschl, U.; Chen, Y.-M.; Dai, D.; Molina, L. T.; Worsnop, D. R.; Kolb, C. E.; Molina, M. J. *J. Phys. Chem. A* **1997**, *101*, 10000–10011.
- (28) Sander, S. P.; Friedel, R. R.; Ravishankara, A. R.; Golde, D. M.; Kolb, C. E.; Kurylo, M. J.; Molina, M. J.; Moortgat, K. G.; Keller-Rudek, H.; Finlayson-Pitts, B. J.; et al. *Chemical Kinetics and Photochemical Data for Use in Atmospheric Studies, Evaluation Number 15*, UPL Publication 06-2, NASA Jet Propulsion Laboratory: Pasadena, California, 2006.
- (29) Creasey, D. J.; Heard, D. E.; Lee, J. D. *Geophys. Res. Lett.* **2000**, *27*, 1651–1654.
- (30) Wine, P. H.; Thompson, R. J.; Ravishankara, A. R.; Semmes, D. H.; Gump, C. A.; Torabi, A.; Nicovich, J. M. *J. Phys. Chem.* **1984**, *88*, 2104–2109.
- (31) Atkinson, R.; Baulch, D. L.; Cox, R. A.; Crowley, J. N.; Hampson, R. F.; Hynes, R. G.; Jenkin, M. E.; Rossi, M. J.; Troe, J. *Atmos. Chem. Phys.* **2004**, *4*, 1461–1738; IUPAC Subcommittee for Gas Kinetic Data Evaluation, <http://www.iupac-kinetic.ch.cam.ac.uk>
- (32) Ivanov, A. V.; Trakhtenberg, S.; Bertram, A. K.; Gershenson, Y. M.; Molina, M. J. *J. Phys. Chem. A* **2007**, *111*, 1632–1637.
- (33) Hanson, D. R.; Eisele, F. L. *J. Phys. Chem. A* **2000**, *104*, 1715–1719.
- (34) Lanzendorf, E. J.; Hanisco, T. F.; Donahue, N. M.; Wennberg, P. O. *Geophys. Res. Lett.* **1997**, *24*, 3037–3038.
- (35) Hinds, W. C. *Aerosol Technology: Properties, Behavior, and Measurement of Airborne Particles*; John Wiley and Sons, Inc.: New York, 1999.
- (36) Reiner, T.; Arnold, F. *J. Chem. Phys.* **1994**, *101*, 7399–7407.
- (37) Sorokin, A.; Katragkou, E.; Arnold, F.; Busen, R.; Schumann, U. *Atmos. Environ.* **2004**, *38*, 449–456.
- (38) Eisele, F. L.; Tanner, D. J. *J. Geophys. Res.* **1991**, *96*, 9295–9308.
- (39) Lovejoy, E. R.; Hanson, D. R.; Huey, L. G. *J. Phys. Chem.* **1996**, *100*, 19911–19916.

- (40) Tanner, D. J.; Jefferson, A.; Eisele, F. L. *J. Geophys. Res.* **1997**, *102*, 6415–6425.
- (41) Mauldin III, R. L.; Tanner, D. J.; Eisele, F. L. *J. Geophys. Res.* **1999**, *104*, 5817–5827.
- (42) Petäjä, T.; Mauldin, R. L. III; Kosciuch, E.; McGrath, J.; Nieminen, T.; Paasonen, P.; Boy, M.; Adamov, A.; Kotiaho, T.; Kulmala, M. *Atmos. Chem. Phys.* **2009**, *9*, 7435–7448.
- (43) Jokinen, T.; Sipilä, M.; Junninen, H.; Ehn, M.; Lönn, G.; Hakala, J.; Petäjä, T.; Mauldin, R. L. III; Kulmala, M.; Worsnop, D. R. *Atmos. Chem. Phys. Discuss.* **2011**, *11*, 31983–32002.